Spectroscopic Properties and Potential Energy Surfaces for Curium Hydrides: CmH_2, CmH_2^+, CmH, and CmH^+†

K. Balasubramanian*,‡,§,∥ and Zhiji Cao‡

College of Science, California State University, East Bay, Hayward, California 94542, Chemistry and Material Science Directorate, Lawrence Livermore National Laboratory, Livermore, California 94550, and Lawrence Berkeley Laboratory, University of California, Berkeley, California 94720

Received: April 24, 2009; Revised Manuscript Received: July 30, 2009

A relativistic complete active space multiconfigurational self-consistent field followed by multireference singles + doubles configuration interaction computations are carried out on the potential energy surfaces of electronic states of CmH_2 and CmH_2^+ for the insertion reaction of Cm and Cm^+ into H_2. We have also carried out corresponding computations on several electronic states of CmH and CmH^+. Moreover, multireference relativistic configuration interaction computations including spin−orbit coupling were carried out on 75 electronic states of CmH^+, which were found to be below the 45 000 cm^{-1} region. We have computed the first ionization energy of Cm as 5.94 eV in excellent agreement with experimental value of 5.99 eV. Our computations reveal barriers for the insertion of Cm and Cm^+ in their ground electronic states into H_2, but once the barriers are surmounted, both Cm + H_2 and Cm^+ + H_2 form stable products. The potential energy curves of CmH and CmH^+ reveal the existence of several low-lying open-shell excited states with varied Λ quantum numbers and spin multiplicities. The excited states of these species exhibit intermediate coupling, although the spin−orbit splittings of the $^9\Sigma^-$ and $^8\Sigma^-$ ground states of CmH and CmH^+ are small, exhibiting nearly inverted multiplets.

1. Introduction

Although considerable efforts have been devoted to actinide migration in the geological and biological environments as well as aqueous chemistry of rare earth complexes,[1−16] there is very little understanding of the gas-phase reaction chemistry of actinide species. Such knowledge of chemical bonding, spectroscopy, reactivity, and electronic structure of these species is vital to our understanding of the nature of actinide interactions and the relative roles of the 5f and 6d orbitals in bonding and reactivity. Such studies are becoming significantly relevant as considerable amounts of high-level nuclear wastes are generated by a variety of nuclear activities, and it is thus of paramount importance to understand the nature of structure and reactivity of actinide complexes and reactivity. Moreover, chemisorption of actinides onto geological minerals would be governed by the nature of chemical bonds between actinides and surfaces of these materials, and thus surface reactions of actinides could provide considerable insight into the role of 5f and 6d orbitals in these interfacial interactions.

Among the nuclear waste products, Cm(III) species exhibit high fluorescence spectroscopic sensitivity, and thus many experimental studies[17−21] have been devoted to the spectroscopy of Cm complexes and other actinides.[16,17,19] Time-resolved fluorescence spectra of some of these actinides with the *Bacillus sphaericus* strain obtained by Panak and Nitsche[16] have revealed remarkable similarities of the spectra with the *B. sphaericus* strain to the spectra of organic and inorganic phosphates, indicating that the primary mode of binding of the actinides to bacteria is through their adenosine phosphate groups.

The gas-phase reactions and chemistry of actinides have received increased attention over the years.[22−42] Armentrout, Beauchamp, and co-workers[25,26,33,34] have pioneered gas-phase reaction studies of U^+ with small molecules such as D_2, CD_4, and N_2, etc. Cornehl, de Matos, and co-workers[31,32,38] have studied the reactions of small molecules with analogous Th^+, ThO^+, U^+, and UO^+. Gibson and co-workers[5,21,24,30,40−42] have carried out experimental studies on the gas-phase reactions of a number of actinides with molecules such as hydrocarbons, D_2, and O_2. As noted by Gibson et al., in a recent paper[24] on Cm reactions with small molecules, the insertion of lanthanide and actinide ions into C−H and H−H bonds is a critical step in reactions of rare earths with hydrocarbons. Such reactions are important in dehydrogenation and cracking processes. There have been several high-temperature thermodynamic studies and experimental studies concerning the aqueous chemistry of Cm(III) compounds.[58−63]

A recent experimental study by Gibson et al.[24] on the reactions of Cm^+ and CmO^+ with alkenes, acetonitrile, and hexafluoropropene has revealed some interesting reactivity trends. On the basis of the observed results, these authors have suggested that Cm^+ is less reactive compared to U^+ primarily due to the $7s^2$ closed-shell of Cm^+. The 6d orbitals expand in these systems and thus provide an avenue for reactivity through the insertion of the metal 6d into the H−H or C−H bonds. Consequently, the relative role of 6d versus 7s and 5f orbitals in the reactivity of these species is critical to shed light into gas-phase chemistry of these species.

Relativistic effects including spin−orbit coupling can play vital roles in the gas-phase chemistry of actinide species,[44−57] as 7s and 7p orbitals undergo relativistic contraction while the 6d orbitals expand their spatial extent due to relativity. These

† Part of the "Russell M. Pitzer Festschrift".

* Corresponding author. E-mail: balu@llnl.gov.
‡ California State University.
§ Lawrence Livermore.
∥ University of California.

10.1021/jp903795q CCC: $40.75
Published on Web 09/08/2009

features could have a dramatic influence on how actinide reactivities contrasted with the corresponding lanthanides. The hydrides and dihydrides are very useful systems from the standpoint of understanding the mechanisms of actinide insertion reactions into H_2. The extent of participation of the 5f, 7s, and 6d orbitals of Cm in hydrogen insertion can also provide insight into other actinide species.

We have carried out high-level relativistic computations that have included electron correlation effects on the potential energy surfaces of several curium hydrides. We have studied the potential energy surfaces for insertion into H_2 as well as diatomic CmH and CmH^+ species. We have also carried out extensive relativistic configuration interaction computations that included spin−orbit coupling on up to 75 electronic states of CmH^+ and have provided spectroscopic information on several excited states of these species.

2. Method and Computational Details

Curium is one of the most complex actinides due to its half-filled 5f and singly occupied 6d orbitals that result in a plethora of electronic states of varied spin multiplicities and spatial symmetries. This combined with a large spin−orbit coupling on curium underscores the complexity of Cm. A large array of electronic states is generated with complex interactions among themselves due to both spin−orbit coupling and electron correlation effects. Excited electronic states arising from curium compounds are thus particularly complex and require extensive computations.

We have studied the potential energy surfaces at the full complete active space MCSCF level that included full configuration interaction among the active space of orbitals. Once the potential energy surfaces were generated, we have carried out multireference single + double configuration interaction computations for a number of electronic states of these species near their equilibrium geometries.

All the calculations were carried out using relativistic effective core potentials (RECPs) that included spin−orbit operators.[69,70] The RECPs replaced 78 core electrons of curium with valence 6s, 6p, 5f, 6d, and 7s electrons retained explicitly in the valence space. We have employed contracted [5s6p4d3f] basis sets after a number of trial computations with other basis sets that included several 5g functions for Cm. We have found that the [5s6p4d3f] basis sets were optimal, and addition of more functions including 5g functions did not alter the results significantly. The equilibrium geometries of these species were optimized using DFT with B3LYP functional,[64,66,68] second-order Møller−Plesset perturbation (MP2),[65] and coupled cluster singles + doubles (CCSD) approaches for a critical comparison of these techniques to gauge the accuracy of the ECPs and basis sets. We have also carried out corresponding computations employing larger Stuttgart basis sets[71,72] with small core 60-electron ECPs for curium. The results of these two sets of ECPs and basis sets are also compared in this work, and we have shown that the use of RECPs with 78 core electrons replaced for Cm provides reliable results consistently. The Van Duijneveldt[73] hydrogen basis set was used for the hydrogen atoms augmented by a set of 2p polarization functions.

The CASSCF computations were carried out in C_{2v} symmetry including the 5f, 6d, and 7s orbitals of Cm and hydrogen 1s orbitals in the active space. The core 6s and 6p orbitals of curium were kept inactive at the CASSCF level in that excitations were not allowed from these orbitals, although they were relaxed as a function of molecular geometry. The MRSDCI computations included several million configurations that resulted from single and double excitations from all CASSCF configurations that have coefficients more than 0.03. Consequently, the MRSDCI computations of the entire potential energy surfaces were feasible only for the diatomic CmH and CmH^+ species. However, as we show by such computations on the entire potential curves of the diatomics, the MRSDCI computations are warranted only for the energy separations as geometries do not change too much at the MRSDCI level. Finally, as reactivities of C and Cm^+ toward H_2 are determined primarily by the ground state potential energy surfaces of these species, we have only optimized these species at the MRSDCI level near the minima and dissociation limits to provide accurate assessment of their stabilities and reactivities in the ground states. Moreover, single-reference based approaches such as the CCSD method work reasonably well for the entire regions of the potential energy surfaces of the ground states as leading configurations, and their coefficients do not change too much in the ground states as a function of the geometry.

The relativistic configuration interaction calculations[76] were carried out for a large number of electronic states. As mentioned earlier, curium exhibits a complex array of electronic states due to the $5f^7 6d 7s^2$ configuration in its neutral state and $5f^7 7s^2$ configuration for the cation.[77,78] The fact that the ground-state ionization takes place from the 6d orbital as opposed to 7s for Cm is due to relativity, which stabilizes the 7s orbital[79] and expands the 6d orbital, thus making it a target for first ionization. We have considered over 75 electronic states for CmH^+ to shed light on spin−orbit coupling for this ion. As there are several Λ_-S electronic states with different Λ quantum numbers and spins, relativistic configuration interaction computations tended to be complex and extensive. As an example, we have shown in Table 1 the list of reference configurations that were included from the various low-lying electronic configurations of CmH^+ for the $\Omega = 0$ state of CmH^+. As can be seen from Table 1, there are 2006 low-lying reference determinants which are all candidates for the treatment of various $\Omega = 0$ states. This requires further discussion. For example, the $\Omega = 0$ states arising from the configuration $2\sigma\ 3\sigma\ 1\delta^2\ 1\pi^2\ 1\phi^2$ are generated[79] by the following expansions

$$(2\sigma\,\alpha\ 3\sigma\,\beta)\ 1\delta^{2+}\alpha\ 1\delta^{2-}\beta\ 1\pi^{1+}\alpha\ 1\pi^{1-}\beta\ 1\phi^{3+}\alpha\ 1\phi^{3-}\beta$$

$$(2\sigma\,\beta\ 3\sigma\,\alpha)\ 1\delta^{2+}\alpha\ 1\delta^{2-}\beta\ 1\pi^{1+}\alpha\ 1\pi^{1-}\beta\ 1\phi^{3+}\alpha\ 1\phi^{3-}\beta$$

When each of the above complex δ, π, and ϕ orbitals is expanded in real space, it yields two electronic configurations per spin orbital, and thus when all six complex spin orbitals are multiplied, we get $2^6 = 64$ reference determinants for each of the two configurations; in all, 128 reference configurations are listed in Table 1 for this case. We have included all of the reference configurations shown in Table 1 for the RCI and allowed single + double excitations from these configurations. The RCI computations of other spin−orbit states such as $\Omega =$ 4, 3, 2, 1, etc., included a compatible set of reference configurations corresponding to Table 1 but chosen with appropriate spins and spatial symmetries so that the net Ω quantum number is for the state under consideration. We obtained 20 roots of each Ω state in the RCI which were then assigned appropriately on the basis of the configurations, and the energy separations of these states were computed.

All CASSCF/MRSDCI/RCI computations were carried out using one of the authors' modified version of ALCHEMY 2002 codes.[75] To carry out the complex multireference RCI required

TABLE 1: Low-Lying Electronic Configurations and the References for the RCI of Ω = 0 States[a]

$1\sigma^2\ 2\sigma\ 3\sigma\ 1\delta^2\ 1\pi^2\ 1\phi^2$	$2\sigma\ 3\sigma$	$1\delta^2$	$1\pi^2$	$1\phi^2$		total number of references
angular momentum	0	0	0	0		128
	1	1	−1	−1		1
	1	−1	1	−1		1
	1	−1	−1	1		1
	−1	−1	1	1		1
	−1	1	−1	1		1
	−1	1	1	−1		1
	0	0	1	−1		8
	0	0	−1	1		8
	1	−1	0	0		16
	−1	1	0	0		16
	1	0	−1	0		16
	−1	0	1	0		16
	1	0	0	−1		16
	−1	0	0	1		16
	0	1	0	−1		8
	0	−1	0	1		8
	0	1	−1	0		8
	0	−1	1	0		8
$1\sigma\ 2\sigma\ 3\sigma\ 1\delta^3\ 1\pi^2\ 1\phi^2$	$1\sigma\ 2\sigma\ 3\sigma$	$1\delta^3$	$1\pi^2$	$1\phi^2$		
angular momentum	j1	j2	j3	j4		6,6,24,24,24,32, 32,6,6,8,8,8
$1\sigma2\sigma3\sigma1\delta^2\pi^3\varphi^2$	$1\sigma2\sigma3\sigma$	$1\delta^2$	$1\pi^3$	$1\phi^2$		
angular momentum	j1	j2	j3	j4		96,96,6,6,6,6, 32,32,2,2,2,2
$1\sigma\ 2\sigma\ 3\sigma\ 1\delta^2\ 1\pi^2\ 1\phi^3$	$2\sigma\ 3\sigma$	$1\delta^2$	$1\pi^2$	$1\phi^3$		
Angular momentum	j1	j2	j3	j4		6,6,8,8,8,8,2,2,
$1\sigma^2\ 2\sigma\ 3\sigma\ 1\delta\ 1\pi^3\ 1\phi^2$	$2\sigma\ 3\sigma$	1δ	$1\pi^3$	$1\phi^2$		
angular momentum	j1	j2	j3	j4		32,32,4,4,4,4
$1\sigma^2\ 2\sigma\ 3\sigma\ 1\delta\ 1\pi^2\ 1\phi^2\ 2\pi$	$2\sigma\ 3\sigma$	1δ	$1\pi^2$	$1\phi^2$	2π	
angular momentum	j1	j2	j3	j4	J5	128,128,8*32, 8*16,4*64,
$1\sigma^2\ 2\sigma^2\ 1\delta^2\ 1\pi^2\ 1\phi^2$	$2\sigma^2$	$1\delta^2$	$1\pi^2$	$1\phi^2$		
angular momentum	j1	j2	j3	j4		64
$1\sigma^2\ 3\sigma\ 1\delta^2\ 1\pi^3\ 1\phi^2$	3σ	$1\delta^2$	$1\pi^3$	$1\phi^2$		
angular momentum	j1	j2	j3	j4		32,32,4*8, 4*2,4*8,

[a] Only for the first electronic distribution, all possible combinations are shown; for the remaining cases, we have abbreviated the angular momenta with four symbols (j1, j2, j3, j4) such that the total adds up to zero, and the corresponding number of combinations are shown in the last column, where *n**m means, m occurs *n* times.

for CmH^+, extensive code modifications and enhancements were made, as treatment of the spin−orbit states of CmH^+ required a large reference space that included 2006 reference configurations. We have also enhanced the RCI code to consider a number of excited states, and in the present case, we have extracted up to 20 roots for each Ω quantum number. All of the DFT/MP2/CCSD calculations were carried out using the GAUSSIAN 03 package of codes.[74]

3. Results and Discussion

A. Large-Core, Small-Core RECPS and Single-Reference Methods. We start our discussions with the validation of the RECPs employed here by first considering the low-lying electronic states of CmH_2 which are predominantly single-reference in character. It should be emphasized the ground states of CmH_2, CmH_2^+, CmH, and CmH^+ are all single-reference in their compositions, as we show by considering multireference methods subsequently. Moreover, most of the high-spin multiples are single-reference in character; that is, the nonet states of CmH^+ and decet states of CmH are predominantly single reference in nature. Thus, it is valid to consider the properties of these states and the round states within single-reference approaches such as B3LYP, MP2, and CCSD methods. These techniques were also used to validate the RECPs and basis sets.

TABLE 2: Comparison of Different ECPS and Methods of CmH_2

electronic states	ΔE (kcal/mol)	θ(H−Cm−H) (°)	r(Cm−H) (Å)
B3LYP/Small Basis Set/78-e RECP			
$^7A_2$	0.00	112.2	2.156
$^9A_2$	0.43	114.3	2.067
$^7B_1$	3.74	105.2	2.149
$^9B_2$	28.18	106.6	2.073
$^9A_1$	33.80	100.6	2.056
$^{11}A_1$	44.38	19.9	2.332
$^{11}B_1$	45.53	19.2	2.413
MP2/Small Basis Set/78-e RECP			
$^9A_2$	0.00	116.2	2.040
$^7A_2$	13.3	113.5	2.046
$^9B_2$	26.4	107.5	2.053
$^{11}B_1$	30.43	18.7	2.400
$^9A_1$	30.71	101.6	2.034
$^9B_1$	42.13	111.3	2.063
$^{11}A_1$	51.51	18.3	2.408
$^7B_1$	58.62	105.3	2.093
CCSD/Small Basis Set/78-e RECP			
$^9A_2$	0.00	114.9	2.060
$^7A_2$	11.29	111.0	2.059
$^9B_2$	22.84	108.5	2.076
$^9A_1$	26.86	102.2	2.059
$^{11}B_1$	30.48	18.4	2.437
$^9B_1$	39.29	114.7	2.098
$^7B_1$	67.17	106.0	2.120
$^7A_1$	62.20	21.0	2.274
$^{11}A_1$	45.75	18.3	2.426
B3LYP/Stuttgart Basis Set/60-e RECP			
$^9A_2$	0.00	109.8	2.007
$^7A_2$	6.06	106.8	1.999
$^9B_2$	23.12	105.4	2.026
$^9A_1$	27.13	97.5	2.008
$^{11}A_1$	39.88	19.8	2.318
$Cm(^9D_2) + H_2(^1\Sigma_g)$	13.68		
$Cm(^9D_2) + 2H(^2S)$	123.45		
MP2/Stuttgart Basis Set/60-e RECP			
$^9A_2$	0.00	108.2	1.971
$^7A_2$	13.5	109.7	1.971
CCSD/Stuttgart Basis Set/60-e RECP			
$^9A_2$	0.00	109.6	1.995
$^7A_2$	11.1	110.2	1.992

Table 2 shows the low-lying electronic states of CmH_2 that we have computed using a number of single-reference electronic structure methods near the optimized geometries for the various states. In Table 2 we have shown the results obtained using different techniques, different basis sets, and two different types of ECPs. As can be seen from Table 2, the use of very small core RECPs with only 60 electrons in the core and including a large basis set that included several 5g functions yielded a bond length of 2.007 Å compared to large-core RECPs (78 electrons in the core) with smaller basis sets which yielded 2.040 Å for the Cm−H distances. Moreover, among the single-reference methods, we do not see large differences in the computed geometries near the minima; that is, bond angles are within 5° of each other and the bond lengths within 0.04 Å. Thus, the main variation among the methods is in the energy separations of the excited electronic states which tend to change considerably at different levels. It is interesting to point out that the B3LYP/Small Basis Set/78-e RECP method is the only method that fails to distinguish nearly degenerate $^7A_2$ and $^9A_2$ states for CmH_2 yielding a lower $^7A_2$ state. However, as can be seen from Table 2, a comparison of the results of the MP2 method or the CCSD method that employed small-core and large-core

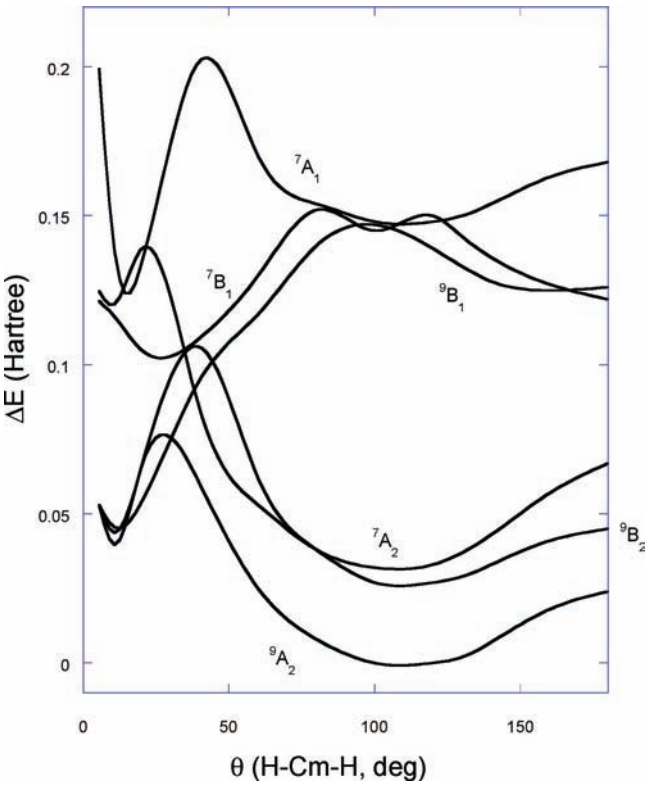

Figure 1. Bending potential energy curves of electronic states of CmH_2 at the CASSCF level, 1 Hartree = 635.6 kcal/mol.

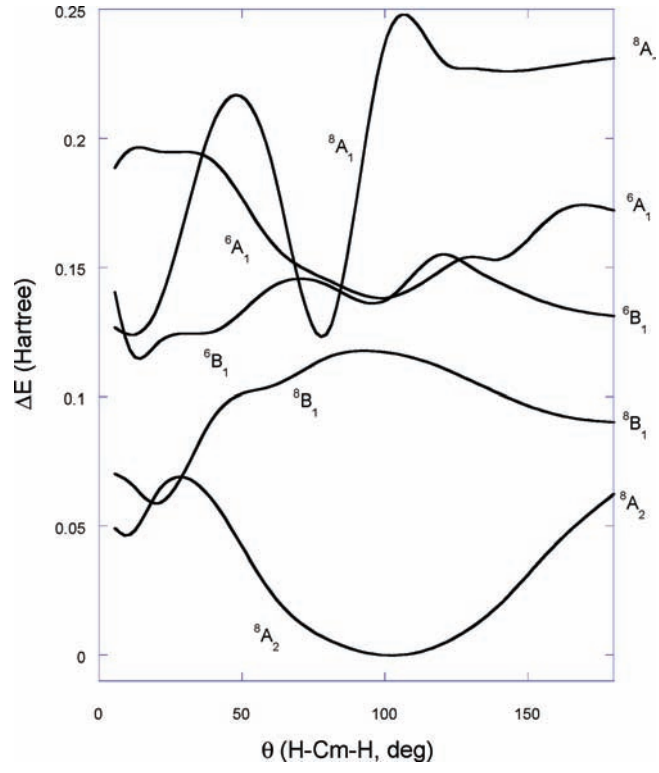

Figure 2. Bending potential energy curves of electronic states of CmH_2 at the CASSCF level.

RECPs reveals that both RECPs yield the same $^9A_2$ ground state. In fact, the computed geometries and energy separations at the MP2 and CCSD levels for the large-core and small-core ECPs are in reasonable agreement providing confidence in the use of large-core RECPs together with the corresponding smaller basis sets compared to the Stuttgart basis sets. The bond distances obtained with the two ECPs for the $^9A_2$ and $^7A_2$ states are within 0.05−0.07 Å; bond angles are within 5°; and the energy separations are within 0.2 kcal/mol of each other at the MP2 level. The CCSD method also yields geometries of comparable accuracy when comparing large-core and small-core ECPs. There is a systematic elongation of Cm−H bond distances by up to 0.07 when large-core RECPs are used. However, the small-core RECPs and the corresponding basis sets are computationally expensive and not well suited for the entire potential energy curves when one employs CASSCF methods. Thus, we use the large-core RECPs uniformly in all studies here.

B. Potential Energy Surfaces and Electronic States of CmH_2 and CmH_2^+. Although single-reference based methods seem to suffice for the ground states of these species at all regions of the potential energy curves, we need to consider the multireference methods for the excited electronic states of these molecules, especially for low spin states. Moreover, the efficacy of single-reference based methods even for the high-spin ground and low-lying electronic states needs to be assessed by consideration of multireference methods. Figure 1 shows the bending potential energy surfaces of eight low-lying electronic states of CmH_2 at the CASSCF level, while the corresponding bending potential energy surfaces for the electronic states of CmH_2^+ are shown on Figure 2. The bending potential energy surfaces provide insight into the energetics for the insertion of the various electronic states of Cm into H_2 in Figure 1 and Cm^+ into H_2 in Figure 2. We have obtained these potential energy surfaces by varying the H−Cm−H bond angle and then fully optimizing the Cm−H bond distance for each bond angle. The optimized energies for each bond angle are then plotted in Figures 1 and 2. The CASSCF computations included full CI within the active space of 5f, 7s, and 6d orbitals, and thus they reproduce all of the qualitative features of the potential energy surfaces, the only exception being the dissociation energies. The dissociation energies and activation energies for the relevant ground states are obtained at the higher MRSDCI level. The maxima on the bending potential energy surfaces are actually saddle points, as they are maxima along minimal energy surfaces (relative to bond distances), and thus the maxima provide the activation energy barriers for the insertion of Cm or Cm^+ into H_2. The CAASCF surfaces do not include external excitations, and thus dynamic electron correlation effects are not included. However, as we show subsequently, by explicit consideration of the potential energy curves of CmH and CmH^+ at the MRSDCI level, the CASSCF method reproduces all of the features such as barriers, minima, and geometries, especially for the ground states of these species. We show that only the dissociation energies are influenced by dynamical electron correlation effects which we have obtained by using the higher-order MRSDCI techniques. Even the activation energy barriers change by only 0.3−0.8 kcal/mol at the MRSDCI level. Consequently, we have used the CASSCF method for the potential energy surfaces and then the MRSDCI method to compute the dissociation energies and the activation energy barriers.

As can be seen from Figure 1 and Figure 2, both CmH_2 and CmH_2^+ exhibit barriers for the insertion into H_2 in their ground electronic states. This finding is consistent with a recent experimental work by Gibson et al.[24] who find that Cm^+ is not reactive toward small closed-shell molecules in the ground state. We have computed the activation energy barrier for the insertion of Cm into H_2 as 20.8 and 20.0 kcal/mol at the CASSCF and MRSDCI levels. The corresponding values for the insertion of Cm^+ into H_2 are 43.9 and 44.2 kcal/mol, respectively. Once

TABLE 3: Computed Low-Lying Bent Electronic States of CmH_2 and CmH_2^+ at the CASSCF and MRSDCI Levels

electronic states	r_e (Cm−H) (Å)	θ(H−Cm−H) (°)	ΔE (kcal/mol)
CmH_2 $^9A_2$[b]	2.059(2.023)	110.8(113)	0.00(0.0)[a]
$^9B_2$	2.095	111.6	16.9(20.5)
$^7A_2$	2.054	107	20.50(19.9)
$^9B_1$	2.117	161.2	78.7(72.7)
$^7B_1$	2.055	115.4	87.6(80.7)
$^7A_1$	2.049	111.6	92.9(82.9)
CmH_2^+ $^8A_2$	1.975(1.96)	102.0(99.8)	126.7(140.0)
$^8B_1$	2.10	180.0	183.9(196.7)
$^8B_1$	2.09	43.2	186(198.5)
$^8A_1$	2.22	80(76)	206(203)
$^6B_1$	2.05(2.03)	180.0	210.4(222.8)
$^6A_1$	1.98(2.00)	180.0	214.6(239.2)
$^6B_1$	1.965	98.5	212.15(221.5)
$^6A_1$	1.949	98.1	214.51(220.7)

[a] The CASSCF and MRSDCI dissociation energies for the ground state of CmH_2 relative to Cm + H_2 are 33.7 and 33.9 kcal/mol, respectively. The dissociation energies at the CASSCF and MRSDCI levels for CmH_2^+ are 31.0 and 30.0 kcal/mol, respectively, relative to $Cm^+ + H_2$. The IP of CmH_2 is computed as 140.0 kcal/mol at the MRSDCI level. [b] Numbers in parentheses are at the MRSDCI level. [c] Even spin multiplets are for CmH_2^+.

the barrier is surmounted, both Cm and Cm^+ form stable bent structures in their ground states. The computed dissociation energies are 33.7 and 33.9 kcal/mol, respectively, for CmH_2. The corresponding dissociation energies at the CASSCF and MRSDCI levels for CmH_2^+ are 31.0 and 30.0 kcal/mol at the CASSCF and MRSDCI levels, respectively, relative to $Cm^+ + H_2$.

Table 3 shows our computed electronic states near the minima at both CASSCF and MRSDCI levels of theory. As can be seen from Table 3, the optimized MRSDCI geometries of the ground states are quite close to the CASSCF equilibrium geometries for the ground states. The MRSDCI Cm−H bond distances are within 0.02−0.05 Å of the CASSCF values and H−Cm−H bond angles are within 2−4° suggesting that the CASSCF method yields good description of the geometries, and errors in geometries from the RECPs are systematically comparable to these differences. The energy separations are more sensitive to higher-order dynamical electron correlation effects. Even so, as can be seen from Table 3, the differences in the energy separations are between 0.6 and 10 kcal/mol (for the high-lying $^7A_1$ state). It is should be noted that for the relevant low-lying states that influence the reactivity the CASSCF method works quite well. This is primarily because the CASSCF used here included a full CI among the most important orbitals of Cm. The multireference techniques are obviously important for the excited low-spin states, but the ground states are predominantly single-configurational. Consequently, although a single-reference method, such as the CCSD method, yields accurate geometries and dissociation energies for the ground state, it does not provide reasonable description of the excited states owing to their multireference characters. For example, the CCSD method yields $r_e = 1.98$ Å and $\theta e = 98.6°$ for the $^8A_2$ ground state of CmH_2^+.

As can be seen from Table 3, the ground state of CmH_2^+ is $^8A_2$ with Cm−H distances of 1.98 Å compared to the $^9A_2$ ground state of CmH_2 which exhibits longer Cm−H distances of 2.059 Å. The shorter Cm−H bond distances for CmH_2^+ are consistent with the electron depletion on Cm which enhances the iconicity of the Cm−H bond compared to the neutral species. Moreover the H−Cm−H bond angle for the cation contracts to 102 from 110.8° for CmH_2. Again the bond contraction is consistent with the cation formation and the nature of hybridization in the cation compared to the neutral species. It should be noted that the neutral Cm has a singly occupied 5d orbital[78] which is unoccupied for Cm^+. There is considerable electron transfer from curium to the hydrogens in both cases resulting in ionic Cm−H bonds. CmH_2 and CmH_2^+ exhibit comparable barriers in their respective ground states, but excited electronic states of Cm and its cation insert into the H_2 bond spontaneously.

In accord with the experimental findings of Gibson et al.,[24] Cm^+ is not reactive toward H_2, and in fact, as noted above, the ground state of CmH_2^+ has to surmount a barrier before the reactants $Cm^+ + H_2$ form the CmH_2^+ ion. This is in contrast to other early actinides such as U, Pu, and U^+.[80−83] Both U and U^+ form very stable hydrides, and their hydride products are formed with smaller activation barriers.[80] Evidently curium ion's different behavior in this regard is attributed to an unoccupied 6d and the enhanced 5f population in the ground state of Cm^+. For the insertion of Cm^+ into H_2, the 6d (σ) orbital participation is critical in both electron transfer from H_2 and back transfer to H_2 from the 6d (π) orbital. The 6d orbitals are higher for Cm^+ and Cm compared to the early actinide metals. As one moves across the actinide period, there is greater influence of relativistic actinide contraction which increases the 5f occupancy and thus decreases the 6d occupancy. Consequently, in the case of the early actinides 6d competes effectively with the 5f orbitals. This is an important factor that governs the reactivity of actinide species across the actinide row and explains why the early actinides are more reactive toward hydrogen compared to the latter actinides in the series.

We have computed the adiabatic ionization energy of CmH_2 to form the ground state of CmH_2^+ at its bent minimum as 140 kcal/mol or 5.99 eV at the MRSDCI level. The corresponding adiabatic IP of CmH_2 at the CCSD level is computed as 142.8 kcal/mol or 6.11 eV. The close agreement between the CCSD IP and MRSDCI adiabatic IP of CmH_2 is fully consistent with the predominantly single-reference characters of the ground states of both CmH_2 and CmH_2^+. We also note that this value is quite close to the experimentally measured IP of 5.99 eV for the Cm atom by Köhler et al.[77] This means the orbital relaxation effects and geometrical changes upon ionization approximately appear to cancel out which each other so that the ionization of the molecule mimics that of the Cm atom. As seen from Table 3, although there is appreciable geometry change upon ionization of CmH_2 (bond length contracts by 0.08 Å and bond angle also contracts by 9°), these changes cancel out with orbital relaxation effects so that we do not see a significant change in the adiabatic IP. However, the geometrical changes that we find in Table 3 upon ionization would result in considerable vibrational progression in the photoelectron spectra of CmH_2.

C. Spectroscopic Constants and Potential Energy Curves of CmH and CmH^+. We have also studied the electronic states and spectroscopic properties of the diatomic CmH and its cation to shed further light into relativistic effects and especially the nature of the excited states of these species. Moreover, spectroscopy of these small molecules is accessible to high-resolution laser spectroscopic studies. Thus we have considered the potential energy curves and spectroscopic properties of CmH and CmH^+. Figure 3 shows the potential energy curves of CmH at the CASSCF level, while the corresponding potential energy curves are shown in Figure 4 for CmH^+. The ground electronic states of the diatomic species are predominantly single-reference in their characters similar to CmH_2 and CmH_2^+, and thus single-reference methods such as the CCSD method yield accurate spectroscopic constants for the ground states. However owing to the multireference natures of the excited electronic states of

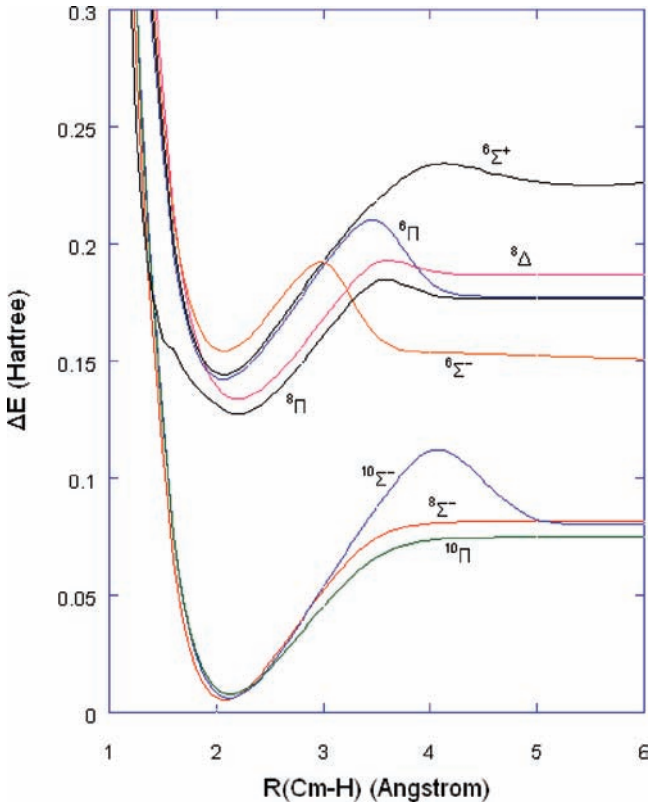

Figure 3. Potential energy curves of low-lying electronic states of CmH at the CASSCF level.

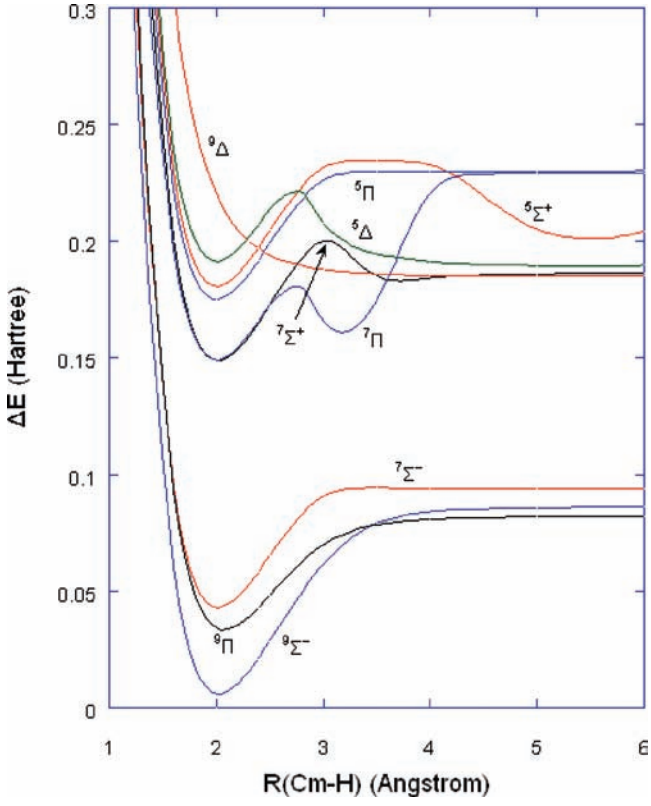

Figure 4. Potential energy curves of low-lying electronic states of CmH^+ at the CASSCF level.

these species, we believe that the CASSCF/MRSDCI approaches are more reliable for the excited states. As can be seen from Figures 3 and 4, there are already a large number of excited electronic states which would split further in the presence of

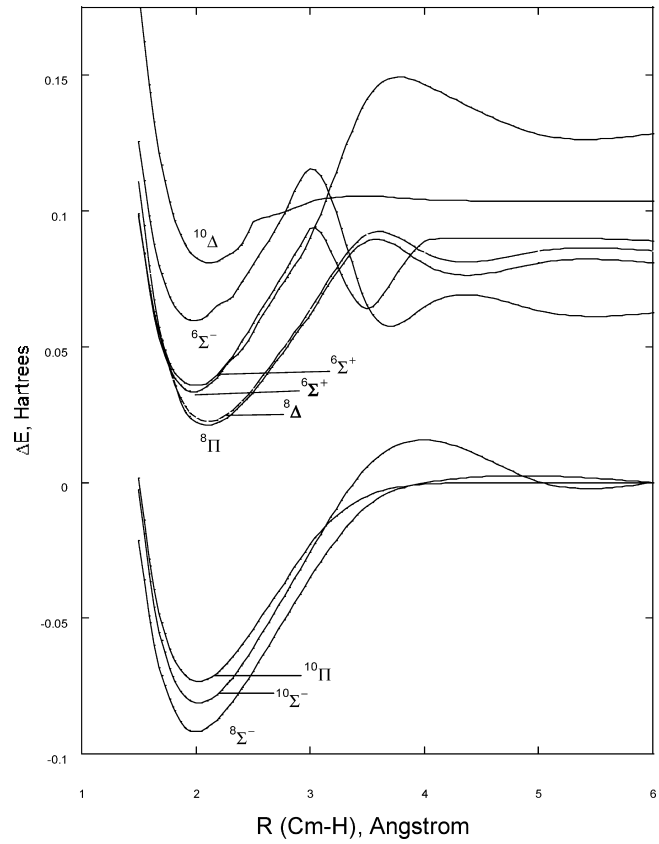

Figure 5. Potential energy curves of low-lying electronic states of CmH at the MRSDCI level.

the spin−orbit operator. Thus, there is a plethora of electronic states for spectroscopic studies of CmH and CmH^+. The crossing of the potential energy curves of some of the electronic states is quite interesting in Figures 3 and 4. The crossing of $^9\Delta$ with several of the potential energy curves of several states in Figure 4 would mean that the $^9\Delta$ state in Figure 4 would predissociate all excited states it crosses. Likewise, as can be seen from Figure 4, the $^5\Delta$ state crosses the potential energy curve of the $^5\Sigma^+$, $^5\Pi$, and $^7\Pi$ curves. The $^8\Sigma^-$ and $^{10}\Sigma^-$, $^{10}\Pi$, and a few other octet and decet states of CmH arise from the Cm(^{9}D) ground state atom, while the first excited manifold of electronic states arises from Cm(^{7}F). Consequently, the $^6\Phi$, $^6\Sigma^-$ excited states correlate into the Cm(^{7}F) + H manifold and result from excitation of an electron from the 6d to 5f orbitals of Cm. It should also be noted that there is a competing low-lying ^{7}D excited state of Cm[78] which also generates additional electronic states. Moreover, due to the relativistic stabilization of the 7p orbitals of Cm, electronic states arising from $5d^77s^27p$ of Cm also contribute substantially to the low-lying excited electronic states of CmH.

Figures 5 and 6 show the computed potential energy curves of CmH and CmH^+ at the MRSDCI level. These MRSDCI computations included multimillion configurations and are thus computationally very intensive compared to the CASSCF computations. As MRSDCI computations include dynamical electron correlation effects, the potential energy curves obtained at this level of theory would provide benchmarks for assessing the efficacy of the CASSCF potential energy surfaces. A critical comparison of Figure 3 with Figure 5 shows that virtually all of the features such as potential minima, the maxima, and dissociation features are well reproduced by the CASSCF method compared to the MRSDCI method. There are only subtle differences between the CASSCF and MRSDCI curves. First,

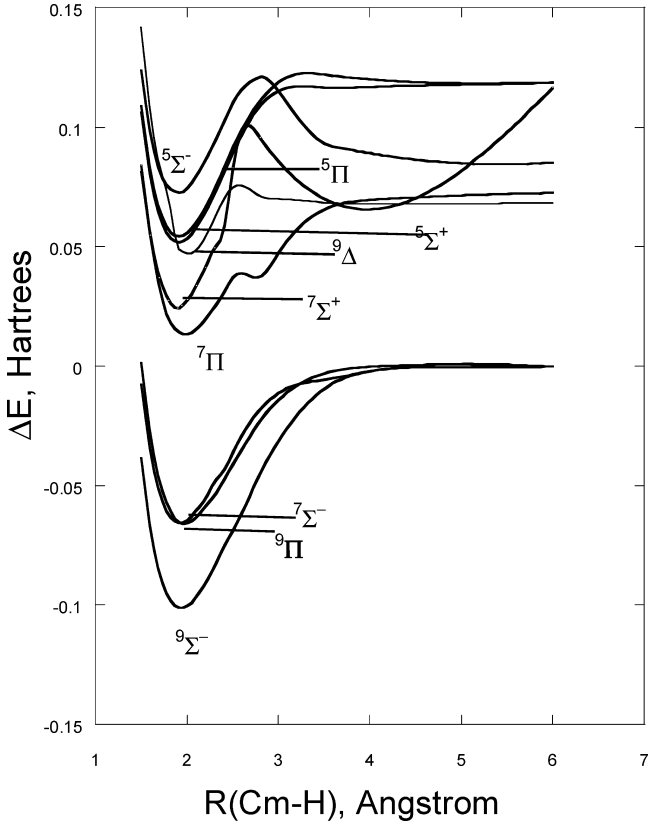

Figure 6. Potential energy curves of low-lying electronic states of CmH^+ at the MRSDCI level.

we see that the potential curves tend to exhibit deeper wells at the MRSDCI level compared to the CASSCF level. Second, the near-degenerate nature of the low-lying electronic states at the CASSCF level is removed at the MRSDCI level. All other features are nicely reproduced by the CASSCF method compared to the MRSDCI method. This is expected as dynamical electron correlation effects that are not included at the CASSCF level tend to stabilize the potential wells to a greater extent, thus resulting in deeper potential wells compared to separated atoms.

Table 4 shows the computed spectroscopic constants for some of the low-lying electronic states of CmH and CmH^+ as obtained by the CASSCF and MRSDCI levels. As can be seen from Table 4, the CASSCF and MRSDCI methods yield very similar results, and even the dipole moments agree quite well. The geometries obtained at the CASSCF level are within 0.004−0.07 Å of each other, and the vibrational frequencies for the low-lying states are also reasonably reproduced. However notable differences are seen for the higher-lying electronic states in both bond distances and vibrational frequencies. Consequently, the dipole moments are also sensitive to the level of theory for the higher-lying electronic states. The dipole moments vary considerably as a function of electronic states; for example, we see a large difference in the dipole moment of the $^8\Sigma^-$ and $^{10}\Sigma^-$ states.

The primary contribution of higher-order electron correlation effects is to the energy separations, as evidenced from Table 4 in comparing the CASSCF and MRSDCI results. For example, the $^8\Sigma^-$ and $^{10}\Sigma^-$ electronic states are nearly degenerate with an energy separation of 0.34 kcal/mol at the CASSCF level, whereas the corresponding MRSDCI energy splitting is 6.75 kcal/mol. We notice a similar trend for other excited electronic levels as well in Table 4. Most of the excited electronic states change by 1−6 kcal/mol, the only exception being the very high-lying $^{10}\Delta$ state (see Table 4).

TABLE 4: Computed Low-Lying Electronic States of CmH and CmH+ at the CASSCF and MRSDCI Levels

system/(method)	electronic states	r(Cm−H) (Å)	T_e (kcal/mol)	ω_e (cm^{-1})	μ_e (D)
CmH(CAS)	$^8\Sigma^-$	2.07	0.00	1759	2.02
CmH(MRCI)	$^8\Sigma^-$	1.996	0.00	1613	1.78
CAS	$^{10}\Sigma^-$	2.060	0.34	1434	3.74
MRCI	$^{10}\Sigma^-$	2.023	6.75	1473	3.54
CAS	$^8\Pi$	2.025	78.28	1863	3.15
MRCI	$^8\Pi$	2.10	71.8	1287	3.43
MRCI	$^8\Delta$	2.107	72.7	1314	3.29
CAS	$^6\Pi$	2.067	86.15	1758	1.99
MRCI	$^6\Pi$	2.027	81.2	1199	1.76
CAS	$^8\Phi$	2.07	96.1		
CAS	$^6\Sigma^-$	2.067	93.51	1764	2.03
MRCI	$^6\Sigma^-$	1.983	96.4	1516	1.82
CAS	^{6}H	2.07	95.5		
CAS	$^6\Gamma$	2.07	97.8		
CAS	$^{10}\Pi$ (2)	2.07	99.9		
CAS	$^8\Sigma^-$ (2)	2.07	139.4		
CAS	$^{10}\Delta$	2.07	177.3		
MRCI	$^{10}\Delta$	2.117	139.4		
CAS	Cm($^9D_2$) + H		51.8		
MRCI	Cm($^9D_2$) + H		60.8		
CmH^+(CAS)	$^9\Sigma^-$[a]	1.959	0	1646	2.93
CmH^+(MRCI)	$^9\Sigma^-$[a]	1.933	0	1716	2.94
MRCI	$^9\Pi$	1.960	22.3	1711	3.20
CAS	$^7\Pi$	2.00	91.3		3.39
MRCI	$^7\Pi$	1.98	72.8	1720	3.57
MRCI	$^7\Pi'$	2.12	68.3		
CAS	$^7\Sigma^-$	1.951	23.6	1643	2.49
MRCI	$^7\Sigma^-$	1.92	22.6	1720	2.45
CAS	$^5\Pi$	1.937	107.4	1650	2.54
MRCI	$^5\Pi$	1.904	98.9	1730	2.45
MRCI	$^9\Delta$	2.00	94.3	1510	2.49
MRCI	$^7\Sigma^+$	1.92	79.7	1724	2.85
CAS	$^5\Sigma^+$	2.00	111.4		2.64
MRCI	$^5\Sigma^+$	1.905	97.3	1735	2.45
CAS	$^5\Delta$	1.945	116.3	1666	2.02
MRCI	$^5\Delta$	1.892	110.6	1708	2.27
CAS	Cm^+ ($^8S_{7/2}$) + H		55.3		
MRCI	Cm^+ ($^8S_{7/2}$) + H		64.3		

[a] The CmH ground state ionization energy at the MRSDCI level is 130.6 kcal/mol. The IP of Cm is 5.83 eV at the MRSDCI level and 5.94 eV corrected for spin−orbit effects, compared to the experimental value of 5.99 eV.

It is important to assess the accuracy of a single-reference based approach such as the CCSD method. Although the ground state of CmH is the $^8\Sigma^-$ state, the first excited $^{10}\Sigma^-$ state is placed at 19 kcal/mol above the ground state at the CCSD level. This energy separation is quite different from the MRSDCI result of 6.8 kcal/mol. However, the Cm−H bond distance at the CCSD level is 2.04 Å compared to the MRSDCI value of 1.996 Å. The CCSD vibrational frequency of the ground state of CmH is 1507 cm^{-1} compared to 1613 cm^{-1} at the MRSDCI level. The CCSD r_e value for the first excited $^8\Sigma^-$ state is 2.062 Å compared to the MRSDCI result of 2.023 Å. As we discuss subsequently, the multiconfiguration treatments provide a different description, especially for the excited electronic states of CmH, as these tend to be highly multireference in character. Thus, sometimes the CCSD and MRSDCI energy differences are substantial; for example, for the $^8\Delta$ state the CCSD method yields an energy separation of 32 kcal/mol, while the corresponding MRSDCI value is 72.7 kcal/mol. Such large differences are noted especially for electronic states for which the principal configuration makes less than 30% contribution.

Table 4 reveals the complexity of interplay between electron correlation effects and multireference characteristics for the high-

lying and some low-lying electronic states of CmH and CmH^+. As can be seen from Table 4, where CmH exhibits nearly degenerate $^8\Sigma^-$ and $^{10}\Sigma^-$ states at the CASSCF level, at the MRSDCI level the $^8\Sigma^-$ state prevails as the ground state, as higher-order dynamical electron correlation effects stabilize the $^8\Sigma^-$ state. We have found several low-lying excited electronic states at both the CASSCF and MRSDCI levels in Table 4, especially for CmH. This is due to the fact that the 6d orbital competes with the 5f orbital for the low-lying electronic states of CmH, whereas in the case of CmH^+ most of the electronic states arise from the occupation of the 5f orbitals. There are two low-lying states of spin multiplicity 10 which are of $^{10}\Sigma^-$ and $^{10}\Pi$ symmetries. As can be seen from Table 4, other electronic states arising from spin multiplicities of 8 and 6 are higher in energy. Most of the excited electronic states exhibit minima near the ground-state geometry. Table 4 reveals that the electronic states of CmH exhibit ionic character with dipole moments ranging from 1.78 to 3.74 D.

The electronic states of CmH^+ are also shown in Table 4, and clearly the $^9\Sigma^-$ state is the ground state of CmH^+, as evidenced from Table 4 at both the CASSCF and MRSDCI levels. Interestingly the $^9\Sigma^-$ ground state is also consistent with the CCSD method which yields $r_e = 1.968$ Å and $\omega_e = 1688$ cm^{-1}. These results agree quite well with the MRSDCI results that we have shown in Table 4 for the ground state. The first excited $^7\Sigma^-$ state of CmH^+ is 22.2 kcal/mol above the ground state at the MRSDCI level, which is consistent with the CCSD value of 19.4 kcal/mol. The higher excited electronic states of both CmH and CmH^+ are highly multireference in their characters, and thus a single-reference based method such as the CCSD method does not yield an accurate description of these states. The dipole moments of CmH^+ are larger compared to CmH, but as is well-known, the dipole moments of charged species are gauge dependent. For the electronic states of CmH^+, the dipole moments were computed by placing the gauge on Cm. The computed vibrational frequencies of the electronic states of CmH and CmH^+ are in the range of 1500−1700 cm^{-1}.

The first adiabatic ionization energy of CmH is computed as 130.6 and 137.4 kcal/mol at the MRSDCI and CCSD levels of theory. We believe that the MRSDCI result is the most accurate, especially for the treatment of excited electronic states of these species. The electronic states of CmH^+ exhibit uniform contraction in the bond distances relative to CmH electronic states due to the removal of the outer 6d electron. This is consistent with an expanded spatial extent of the 6d orbital of Cm due to relativistic destabilization of the 6d orbital.

The first ionization energy of the Cm atom has been measured experimentally by Köhler et al.,[77] as 48 324 cm^{-1} or 5.99 eV. We have deduced the ionization energy of Cm from our MRSDCI computations by finding the energy separation of Cm + H and Cm^+ + H at the dissociation limits of the respective ground electronic states. The MRSDCI result obtained in this manner is 5.83 eV. However, this value needs to be corrected for spin−orbit coupling. The ground state of Cm is a bit more stabilized by spin−orbit effects due to its $5f^7 7s^2 6d^1$ configuration compared to the $5f^7 7s^2$ configuration of Cm^+. The presence of an extra electron in the 6d orbital of Cm compared to Cm^+ is expected to result in spin−orbit stabilization of the Cm atom relative to Cm^+, and thus the first ionization energy of Cm is obtained as 5.95 eV including spin−orbit effects, in excellent agreement with the experimentally measured value of 5.99 eV for the first ionization of Cm.

We have computed the dissociation energy of the CmH ground state as 51.8 kcal/mol at the CASSCF level, while the corresponding MRSDCI value is 60.8 kcal/mol. Moreover, we note that the spin−orbit effects approximately cancel out in the D_e computation, as the open-shell characters of the Cm and CmH ground states are preserved, and moreover, the 5f Mulliken population is nearly the same for the molecule and the dissociated species. The spin−orbit effects of the low lying electronic states of CmH are predominantly determined by the 5f shell's spin−orbit coupling of the Cm atom. Consequently, we believe that the MRSDCI D_e of 60.8 kcal/mol should be considered quite accurate to within a few kcal/mol of the experimental result. As can be seen from Table 4, a similar trend emerges in comparing the dissociation energy of the CmH^+ ion at the CASSCF and MRSDCI levels. Whereas the D_e is 55.3 kcal/mol at the CASSCF level, it becomes 64.3 kcal/mol at the MRSDCI level. Consequently, the largest contribution by dynamical electron correlation effects is to the dissociation energies of these species. Another important result is that CmH^+ is more stable than CmH which is primarily attributed to the fact that the ionization process leads to considerable orbital relaxation and rearrangement of electron density. In particular, although the ionization of a separated Cm atom takes place primarily at the 6d orbitals, the CmH molecule exhibits a different behavior. The rearrangement of electron density results in a decrease of charge density of the 7s orbital, whereas the 6d charge remains nearly the same for CmH and CmH^+. This is accompanied by the Cm−H bond contraction for the cation.

TABLE 5: Leading Configurations for the Electronic States of CmH_2, CmH_2^+, CmH, and CmH^+

system	electronic states	leading configurations	weight
CmH_2	$^9A_2$	$1a_1^2 2a_1^1 3a_1^1 4a_1^1 1b_2^2 2b_2^1 3b_2^1 1b_1^1 2b_1^1 1a_2^1$	95%
	$^9B_2$	$1a_1^2 2a_1^1 4a_1^1 1b_2^1 2b_2^1 3b_2^2 1b_1^1 2b_1^1 3b_1^1 1a_2^1$	95%
	$^7A_2$	$1a_1^2 3a_1^2 4a_1^1 1b_2^2 2b_2^1 3b_2^1 1b_1^1 2b_1^1 1a_2^1$	57%
	$^9B_1$	$1a_1^2 2a_1^2 3a_1^1 4a_1^1 1b_2^1 2b_2^1 3b_2^1 1b_1^1 2b_1^1 1a_2^1$	91%
	$^7A_1$	$1a_1^2 2a_1^1 3a_1^1 4a_1^1 1b_2^2 2b_2^1 1b_1^1 2b_1^2 1a_2^1$	52%
CmH_2^+	$^8A_2$	$1a_1^2 2a_1^1 3a_1^1 1b_2^2 2b_2^1 3b_2^1 1b_1^1 2b_1^1 1a_2^1$	94%
	$^8A_1$	$1a_1^2 2a_1^1 3a_1^1 1b_2^2 2b_2^1 1b_1^1 2b_1^1\ 3b_1^1\ 1a_2^1$	55%
		$1a_1^2 2a_1^1 3a_1^1 3b_2^2 2b_2^1 1b_1^1 2b_1^1\ 3b_1^1\ 1a_2^1$	
	$^8B_1$	$1a_1^2 2a_1^1 1b_2^2 2b_2^2 3b_2^1 1b_1^1\ 2b_1^1\ 1a_2^1$	34%
		$1a_1^2 2a_1^1 3a_1^1 1b_2^2 2b_2^1 1b_1^1 2b_1^1\ 1a_2^1$	16%
	$^6B_1$	$1a_1^2 2a_1^1\ 1b_2^2 2b_2^2 3b_2^1 1b_1^1\ 2b_1^1\ 1a_2^1$	34%
		$1a_1^2 2a_1^2 3a_1^1\ 1b_2^2 2b_2^1 3b_2^1 1b_1^1 2b_1^1\ 1a_2^1$	16%
	$^6A_1$	$1a_1^2 2a_1^1\ 3a_1^1\ 1b_2^2 2b_2^1 1b_1^2\ 2b_1^1\ 1a_2^1$	31%
		$1a_1^2 2a_1^1 1b_2^2 2b_2^1 3b_2^1 1b_1^1 2b_1^1\ 1a_2^2$	18%
CmH	$^8\Sigma^-$	$1\sigma^2 2\sigma^2 3\sigma^1 1\pi^2 1\phi^2 1\delta^2$	96%
	$^{10}\Sigma^-$	$1\sigma^2 2\sigma^1 3\sigma^1 4\sigma^1 1\pi^2 1\phi^2 1\delta^2$	96%
	$^{10}\Pi$	$1\sigma^2 2\sigma^1 3\sigma^1 1\pi^2 2\pi^1 1\phi^2 1\delta^2$	96%
	$^8\Pi$	$1\sigma^2 2\sigma^2 1\pi^2 2\pi^1 1\phi^2 1\delta^2$	96%
	$^8\Delta$	$1\sigma^2 2\sigma^2 3\sigma^1 1\pi^2 2\pi^1 1\phi^1 1\delta^2$	69%
	$^6\Pi$	$1\sigma^2 2\sigma^2 1\pi^2 1\phi^3 1\delta^2$	59%
	$^6\Sigma^+$	$1\sigma^2 2\sigma^2 3\sigma^1 1\pi^2 1\phi^2 1\delta^2$	55%
	$^6\Sigma^-$	$1\sigma^2 2\sigma^2 3\sigma^1 1\pi^2 1\phi^2 1\delta^2$	59%
CmH^+	$^9\Sigma^-$	$1\sigma^2 2\sigma^1 3\sigma^1 1\pi^2 1\phi^2 1\delta^2$	96%
	$^9\Delta$	$1\sigma^1 2\sigma^1 3\sigma^1 1\pi^2 1\phi^2 1\delta^3$	96%
	$^7\Sigma^-$	$1\sigma^2 2\sigma^1 3\sigma^1 1\pi^2 1\phi^2 1\delta^2$	54%
	$^5\Delta$	$1\sigma^2 2\sigma^1 1\pi^2 1\phi^2 1\delta^2 2\delta^1$	36%
	$^9\Pi$	$1\sigma^1 2\sigma^1 3\sigma^1 1\pi^3 1\phi^2 1\delta^2$	95%
	$^5\Sigma^+$	$1\sigma^2 2\sigma^2 1\pi^2 1\phi^2 1\delta^2$	33%
	$^7\Pi$	$1\sigma^2 2\sigma^1 1\pi^3 1\phi^2 1\delta^2$	44%
	$^5\Pi$	$1\sigma^2 2\sigma^2 1\pi^3 1\phi^2 1\delta$	16%
		$1\sigma^2 2\sigma^1 1\pi^3 1\phi^2 1\delta^2$	16%
	$^7\Sigma^+$	$1\sigma^2 2\sigma^1 3\sigma^1 1\pi^2 1\phi^2 1\delta^2$	59%

D. Nature of Electronic States of CmH, CmH^+, CmH_2, and CmH_2^+. Table 5 shows the leading configurations of the various electronic states of the molecules and ions that we have considered in this study. As can be seen from Table 5, the ground states of both CmH_2 and CmH_2^+ are predominantly

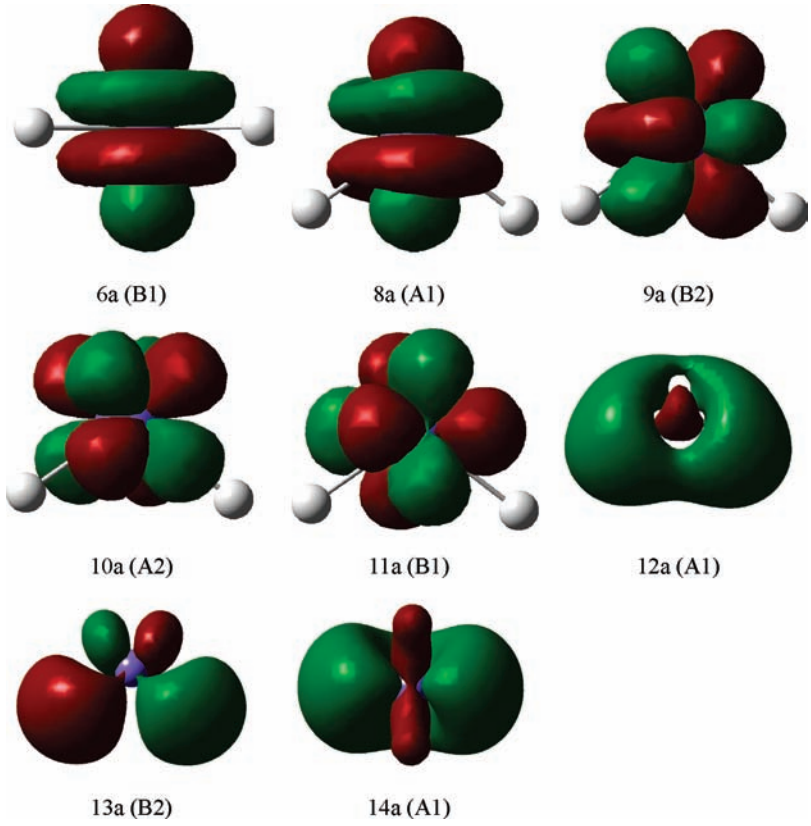

Figure 7. Singly occupied MOs of the ground state ($^9A_2$) of CmH_2. Isodensity was set to be 0.02 for surfaces. MOs are rotated for a better perspective. Symmetries are given in parentheses.

single-reference in character with lead configuration contributing 95% and 94% for CmH_2 and CmH_2^+, respectively. This clearly supports why single-reference based methods such as the CCSD method work well for the ground states of these species. Further analysis of the leading configurations as a function of the bond angle along the bending potential energy surface shows that for the ground states of CmH_2 and CmH_2^+ the dominant configuration remains the same. For example, the coefficient of the leading configuration is 0.977 at the dissociation limit, 0.967 at the minimum, and 0.968 at the barrier. Consequently, we believe that the CASSCF potential energy curves offer very good insight into the reactivity of Cm and Cm^+, especially in the ground electronic states. The ground electronic states of CmH and CmH^+ also exhibit a similar composition as seen from Table 5.

The excited electronic states of all of the species considered here, especially the low-spin states, exhibit very complex multireference characteristics as evidenced from Table 5. In fact, the compositions vary considerably as a function of the geometry, thus explaining the unusual shapes of the excited potential energy curves in Figures 1−4. This is also applicable to the diatomic species CmH and CmH^+ as can be seen both from Table 5 and Figures 3−6. The compositions of these states correlate well with the shapes of the potential energy curves in the figures suggesting that some of the excited states undergo avoided crossings as a function of geometries. This is also confirmed by the fact that the lower spin states are truly multiconfigurational, as can be seen from Table 5. It is evident from Table 5 that with the exception of the high-spin decet and octet states of CmH and the corresponding nonet states of CmH^+ most of the excited states of these species are multiconfigurational.

We can get further into the nature of bonding and electronic states by consideration of the Mulliken populations. The ground state of CmH exhibits Cm Mulliken populations of $5f^{7.0}7s^{1.8}6d^{0.8}7p^{0.2}$. Thus, there is about 0.18e charge transferred from Cm to H to result in partially ionic Cm^+-H^- bond. The populations of most of the low-lying states are nearly the same as all of these states arising from the same state of Cm. The charge transfer is also nearly the same, and consequently, differences in the dipole moments of low-lying electronic states arise from the differences in bond lengths. All states of CmH exhibit populations near 7.0 for the 5f, whereas 6d, 7s, and 7p populations vary. The 7p populations of most electronic states of CmH are between 0.1 and 0.3 due to the relativistic stabilization of the 7p orbitals of Cm and as a consequence of 7p hybridizing with 6d and 7s in the MOs.

The Mulliken populations for the $^9\Sigma^-$ ground state of CmH^+ are $5f^{7.0}7s^{1.87}7p^{0.07}$, suggesting that the ionization of CmH takes place with no change in the 5f populations due to the enhanced stability of the half-filled $5f^7$ shells of Cm. All of the ionization takes place from the 6d orbital of Cm similar to the ionization of the Cm atom. The first excited $^7\Sigma^-$ electronic state of CmH^+ exhibits $5f^{7.0}7s^{1.83}7p^{0.13}$, and thus the variations in Mulliken populations are very small among the low-lying electronic states. The H atom is nearly neutral with an overall gain of 0.05e, and thus the Cm atom has a charge of 0.95 in the ground state of CmH^+. The first excited electronic state also exhibits similar charges on Cm and H. All the trends discussed here for CmH and CmH^+ are similar to CmH_2 and CmH_2^+ except that due to the presence of two hydrogen atoms the charge transfer from Cm to each hydrogen atom to the same extent results in a doubling of the loss of electron density on Cm for CmH_2 compared to CmH.

We have shown in Figures 7−9 the singly occupied orbitals for CmH_2, CmH_2^+, and CmH in their ground electronic states. As can be seen from Figures 7 and 8, all of these open-shell MOs arise from the Cm orbitals with little contributions from

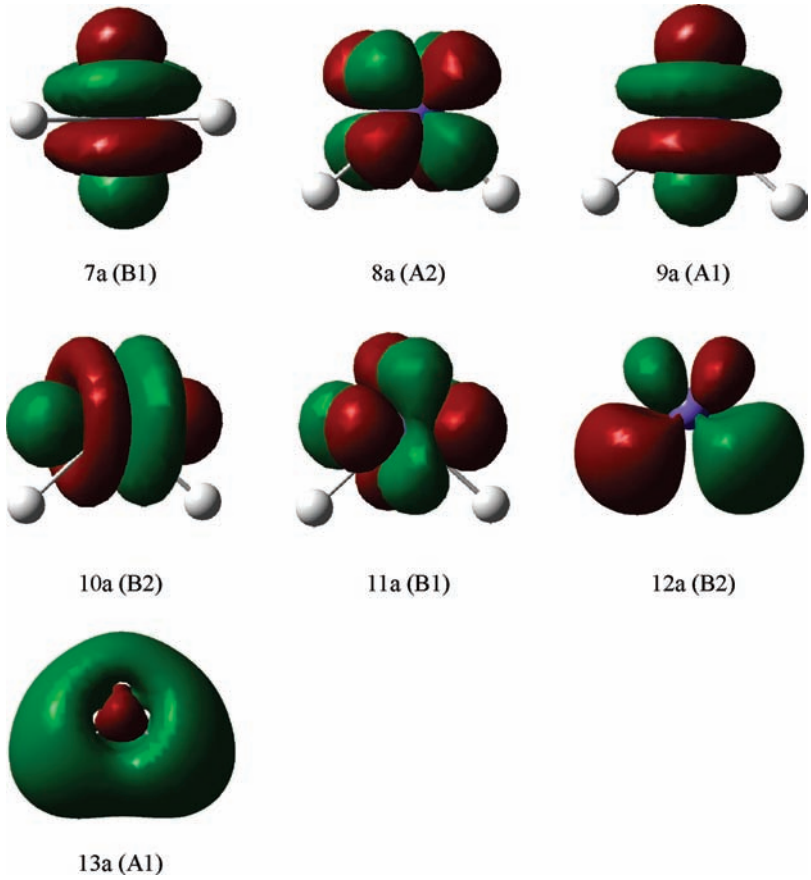

Figure 8. Singly occupied MOs of the ground state ($^8A_2$) of CmH_2^+. Isodensity was set to be 0.02 for surfaces. MOs are rotated for a better perspective. Symmetries are given in parentheses.

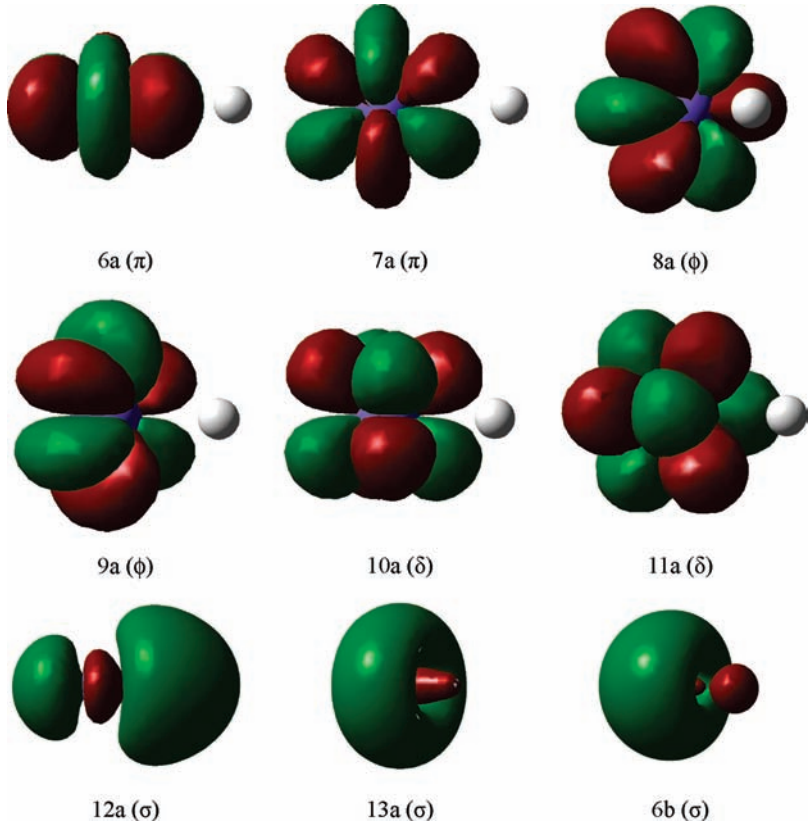

Figure 9. Singly occupied MOs of the ground state ($^8\Sigma$) of CmH. Isodensity was set to be 0.02 for surfaces. MOs are rotated for a better perspective. Symmetries are given in parentheses.

hydrogens in these MOs. This clearly demonstrates that the electronic spin multiplets and spin−orbit components for the lowest-lying states of these species strongly correlate with the Cm ($5f^7$) open-shell character. These orbitals are composed predominantly of the 5f orbitals of Cm. Figure 9 shows the corresponding orbitals of CmH which also confirm that these MOs are composed of the 5f and 6d orbitals of Cm.

E. Spin−Orbit Effects of Electronic States of CmH, CmH^+, CmH_2, and CmH_2^+. Table 6 shows our computed results of the electronic states of CmH^+ including spin−orbit effects as obtained from the RCI computation that included spin−orbit coupling and excitations from up to 2006 reference configurations. As can be seen from Table 6, the electronic states of CmH^+ are quite complex and do not follow any definitive patterns due to the intermediate coupling nature of the spin−orbit states. The electronic states are coupled both by electron correlation effects and spin−orbit effects, particularly in the excited states. Also, Hund's third rule does not hold for these open-shell 5f states, as the 5f orbitals are half-filled. The spin−orbit effects approximately vary with the total Λ values, with the Σ states exhibiting the smallest splitting. However, in excited electronic states due to several other states in the region, spin−orbit effects and correlation effects are strongly coupled. This is clear from Table 6 which shows about 10 roots of each of the Ω quantum numbers. Evidently, due to the intermediate nature of the coupling of electronic states, the higher-lying excited states of CmH^+ are complex mixtures of different states and cannot be ascribed to a particular $\Lambda-S$ state clearly indicating the strong intermediate character. However, the lowest $\Omega = 4$, 3, 2, 1, and 0 spin−orbit components all arise predominantly from the $^9\Sigma^-$ $\Lambda-S$ state. As expected, the splitting for the Σ^- states is smaller, and in this case, it is about 578 cm^{-1} from the lowest $\Omega = 4$ to the highest $\Omega = 1$ states of $^9\Sigma^-$. Likewise, the spin−orbit states in the region 10 478−10 698 cm^{-1} in Table 6 arise from the $^7\Sigma^-$ states. Both states exhibit approximately inverted multiplets. As can be seen from Table 6, we have found more than 50 electronic states above the 22 000 cm^{-1} region, and thus there is a considerable scope for the spectroscopic investigations of the excited states of CmH^+. On the basis of our RCI results on CmH^+, we can make a few inferences on the electronic states of CmH. The $^8\Sigma^-$ state of CmH would split into $\Omega = 7/2$, 5/2, 3/2, and 1/2 components with splitting fully comparable to CmH^+. Consequently, it is predicted that the splittings among these states would be less than 500 cm^{-1}. The $^{10}\Sigma^-$ state of CmH would split into $\Omega = 9/2$, 7/2, 5/2, 3/2, and 1/2 components. The other higher Λ electronic states of CmH would exhibit intermediate coupling and strong mixing with other states that yield the same Ω quantum numbers. It is evident that the higher-lying excited states of CmH are considerably more complex.

Yang and Pitzer[84] have carried out spin−orbit CI studies on the electronic states of EuH. Although EuH is a lighter analogue of CmH^+ and thus is not likely to expect much similarity to CmH^+, it would be interesting to compare our findings. Unlike actinide species, the spin−orbit couplings of lanthanide compounds can be considered within their $\Lambda-S$ manifolds, as mixing with other $\Lambda-S$ states is considerably smaller for the lanthanide compounds. Yang and Pitzer[84] have fit their spin−orbit CI results for EuH into the following nice patterns for the low-lying states.

$$E = T_e + A_e\Sigma + \alpha_e\Sigma^2$$

TABLE 6: Electronic States of CmH^+ Including Spin-Orbit Effects[a]

Ω	T_e
4	0
3	213
2	106
1	578
0	489
3(2)	10478
2(2)	10606
1(2)	10726
0(2)	10698
1(3)	22141
1(4)	27531
3(3)	28494
4(2)	28331
2(3)	28472
3(4)	30436
1(5)	30799
2(4)	30992
1(6)	32082
0(3)	33591
2(5)	33593
3(5)	33813
2(6)	33983
0(4)	33997
3(6)	34215
4(3)	35033
6	35259
1(7)	35615
3(7)	35768
2(7)	35983
0(5)	36124
1(8)	36151
2(8)	36274
1(9)	36274
3(8)	36278
(6)	36605
3(9)	36984
1(10)	37291
2(9)	37504
2(10)	37688
0(7)	37707
1(11)	37736
3(10)	37997
2(11)	38180
1(12)	38195
4(4)	38370
3(11)	38089
3(12)	38309
0(8)	39570
2(12)	39666
3(13)	40160
4(5)	40192
4(6)	41301
0(9)	41527
0(10)	41627
0(11)	42336
4(7)	42692
0(12)	43058
0(13)	43835
0(14)	43991
0(15)	44943

[a] Numbers in parentheses designate upper roots.

where the T_e, A_e, and α_e values were obtained by a fit of their spin−orbit CI results. On the basis of these fits, Yang and Pitzer[84] have obtained $T_e = 0$, $A_e = 0$, and $\alpha_e = -4.19$, with $\Sigma = 0$, 1, 2, 3, and 4 for the $^9\Sigma^-$ state. The fit suggests a very small spin−orbit splitting among the components of the $^9\Sigma^-$ state. Likewise, the $^7\Sigma^-$ state of EuH, which was found to be

about 2231 cm^{-1} higher, exhibited $T_e = 2231$, $A_e = 0$, and $\alpha_e = -2.047$ values with $\sigma = 0, 1, 2, 3$. The negative values of α_e parameters for both states suggest inverted order for the spin−orbit components of EuH, a trend that we also find for CmH^+. However, due to mixing with other electronic states, we do not obtain a strictly inverted multiplet for the low-lying spin−orbit states of CmH^+.

We finally discuss the spin−orbit effects on the dissociation energies, ionization energies, and activation energy barriers. The MRSDCI method without spin−orbit effects yields dissociation energies of 60.8 and 66.5 kcal/mol, respectively, for CmH and CmH^+. The spin−orbit effects are somewhat smaller due to the cancellation of the spin−orbit stabilization at the minimum and dissociation limits, although at the dissociation limit, the spin−orbit effect is slightly more. The spin−orbit effects lower the D_e by 1.5 kcal/mol for the two species, and thus the dissociation energies including spin−orbit effects are 60 and 65 kcal/mol, for CmH and CmH^+, respectively. The adiabatic ionization energies of CmH and CmH_2 including spin−orbit effects are 133 and 142 kcal/mol, respectively. The spin−orbit effects of CmH and CmH_2 are comparable because the 5f and 6d populations are nearly the same in the respective ground states. The same comment applies comparing the spin−orbit effects of CmH_2^+ with CmH^+. As we can see from the potential energy surface of the ground state of CmH_2^+ although Cm^+ forms a stable product when reacted with H_2, it needs to surpass a barrier for the insertion into H_2. That is, although the ground state of the CmH_2^+ ion is 49.0 and 45.5 kcal/mol, more stable at the CASSCF and MRSDCI levels, respectively, compared to the dissociated $Cm^+ + H_2$ species, it has to surpass a barrier of about 44.2 kcal/mol. The barrier does not lower by more than 0.5 kcal/mol by spin−orbit coupling mainly due to the comparable nature of the 5f occupancy near the barrier and the potential minimum. The neutral Cm has to surpass a barrier of 20 kcal/mol, before it forms a stable CmH_2 ground state. The lower barrier for the insertion of Cm into H_2 compared to Cm^+ is because of the occupied 6d orbital in the case of neutral Cm, while the cation has no occupied 6d. The dissociation energies including the spin−orbit effects for CmH_2 and CmH_2^+ are 33.3 and 29.3 kcal/mol, respectively. The stability of CmH_2 is comparable to that of CmH_2^+, but CmH_2^+ is about 4 kcal/mol less stable than CmH_2. The existence of barriers for the insertion of Cm into H_2 both in its neutral and ionic forms confirms the experimental observation of Gibson et al.[24] who have predicted that Cm should be less reactive compared to early actinides such as U and Pu.[80−83]

4. Conclusions

CASSCF/MRSDCI computations carried out here on several curium hydrides reveal that the insertion reactions of Cm and Cm^+ into H_2 need to surmount activation energy barriers of 20 and 44.2 kcal/mol, respectively, making curium less reactive compared to the early actinides. These findings are consistent with the recent experimental gas-phase reactivity studies[24] of Cm^+ with several closed-shell molecules which revealed that curium is less reactive compared to Th^+, U^+, and Pu^+. We have also carried out relativistic computations on several low-lying electronic states of CmH and CmH^+. Such computations including spin−orbit coupling revealed the existence of more than 75 electronic states of CmH^+ that are found to be below 45 000 cm^{-1}. Our computed first ionization energy of Cm of 5.94 eV is in excellent agreement with the experimental value of 5.99 eV reported by Köhler et al.[77] We have found that for both CmH_2 and CmH_2^+, once the barriers in the ground potential energy surfaces are surmounted, $Cm + H_2$ and $Cm^+ + H_2$ form stable CmH_2 and CmH_2^+ products. Our computed potential energy curves for CmH and CmH^+ reveal the existence of several low-lying open-shell excited states with varied Λ quantum numbers and spin multiplicities. Although the ground states $^9\Sigma^-$ and $^8\Sigma^-$ of CmH and CmH^+ exhibit relatively small spin−orbit splittings characterized approximately by inverted multiplets, the excited electronic states not only exhibit multiconfigurational characters but also are intermediately coupled by spin−orbit effects. The first IPs of CmH and CmH_2 are computed as 133 and 142 kcal/mol with spin−orbit corrections included. The dissociation energies of CmH and CmH^+ are computed as 60.8 and 66.5 kcal/mol, respectively. The electronic states of both CmH and CmH^+ exhibit strong ionic characters with Cm^+-H^- polarities.

Acknowledgment. This research was supported by the U.S. Department of Energy under Grant No. DE-FG02-04ER15546. The work at LLNL was performed under the auspices of US Department of Energy. The authors would like to acknowledge computational support on Lawrence Livermore's supercomputer comprising 992 processors supported by DOE's accelerated supercomputing initiative program.

References and Notes

(1) Lombardi, J. R.; Davis, B. *Chem. Rev.* **2002**, *102*, 2431.
(2) Szabo, Z.; Toraishi, T.; Vallet, V.; Grenthe, I. *Coord. Chem. Rev.* **2006**, *250*, 784.
(3) Clark, D. L.; Hobart, D. E.; Neu, M. P. *Chem. Rev.* **1995**, *95*, 25.
(4) Clark, D. L.; Conradson, S. D.; Keogh, D. W.; Palmer, P. D.; Scott, B. L.; Tait, C. D. *Inorg. Chem.* **1998**, *37*, 2893.
(5) Gibson, J. K. *Int. J. Mass Spectrom.* **2002**, *214*, 1.
(6) Kim, J. I.; Freeman, A. J.; Keller, C. *Handbook of the Chemistry and Physics of Actinides*; Elsevier: Amsterdam, 1986.
(7) Danesi, P. R.; Bleise, A.; Burkart, W.; Cabianca, T.; Campbell, M. J.; Makarewicz, M.; Moreno, J.; Tuniz, C.; Hotchkis, M. *J. Environ. Radioact.* **2003**, *64*, 121.
(8) Nitsche, H.; Silva, R. J. *Radiochim. Acta* **1996**, *72*, 65.
(9) Allen, P. G.; Bucher, J. J.; Clark, D. L.; Edelstein, N. M.; Ekberg, S. A.; Gohdes, J. W.; Hudson, E. A.; Kaltsoyannis, N.; Lukens, W. W.; Neu, M. P.; Palmer, P. D.; Reich, T.; Shuh, D. K.; Tait, C. D.; Zwick, B. D. *Inorg. Chem.* **1995**, *34*, 4797.
(10) Allen, P. G.; Shuh, D. K.; Bucher, J. J.; Edelstein, N. M.; Reich, T.; Denecke, M. A.; Nitsche, H. *Inorg. Chem.* **1996**, *35*, 784.
(11) Christ, C. L.; Clark, J. R.; Evans, H. T. *Science* **1955**, *121*, 475.
(12) Apelman, D. *Geol. Soc. Am. Bull.* **1956**, *67*, 1666.
(13) Coda, A.; Dellagiusta, A.; Tazzoli, V. *Acta Crystallogr. B.* **1981**, *37*, 1496.
(14) Blake, C. A.; Coleman, C. F.; Brown, K. B.; Hill, D. G.; Lowrie, R. S.; Schmitt, *J. Am. Chem. Soc.* **1956**, *78*, 5976.
(15) Paramonova, V. I.; Nikolskii, B. P.; Nikolaeva, N. M.; Russ, J. *J. Inorg. Chem.* **1962**, *7*, 528.
(16) Panak, P. J.; Nitsche, H. *Radiochim. Acta* **2001**, *89*, 499.
(17) Moll, H.; Stumpf, T.; Merroun, M.; Rossberg, A.; Selenska-Pobell, S.; Bernhard, G. *Environ. Sci. Technol.* **2004**, *38*, 1455.
(18) Sidorov, L. N. *Int. J. Mass Spectrom. Ion Process.* **1992**, *118*, 739.
(19) Moll, H.; Geipel, G.; Bernhard, G. *Inorg. Chim. Acta* **2005**, *358*, 2275.
(20) Milman, V.; Winkler, B.; Pickard, C. J. *J. Nucl. Mater.* **2003**, *322*, 165.
(21) Smith, P. K.; Peterson, D. E. *J. Chem. Phys.* **1970**, *52*, 4963.
(22) Gibson, J. K.; Haire, R. G. *J. Phys. Chem.* **1990**, *94*, 935.
(23) Gibson, J. K.; Haire, R. G. *J. Phys. Chem. A* **1998**, *102*, 10746.
(24) Gibson, J. K.; Haire, R. G.; Santos, M.; de Matos, A. P.; Marcalo, J. *J. Phys. Chem. A* **2008**, *112*, 11373.
(25) Armentrout, P.; Hodges, R.; Beauchamp, J. L. *J. Am. Chem. Soc.* **1977**, *99*, 3162.
(26) Armentrout, P. B.; Hodges, R. V.; Beauchamp, J. L. *J. Chem. Phys.* **1977**, *66*, 4683.
(27) Heinemann, C.; Cornehl, H. H.; Schwarz, H. *J. Organomet. Chem.* **1995**, *501*, 201.
(28) Marcalo, J.; Leal, J. P.; deMatos, A. P. *Int. J. Mass Spectrom.* **1996**, *157*, 265.
(29) Marcalo, J.; deMatos, A. P.; Evans, W. J. *Organometallics* **1997**, *16*, 3845.
(30) Gibson, J. K. *Organometallics* **1997**, *16*, 4214.

(31) Marcalo, J.; Leal, J. P.; deMatos, A. P.; Marshall, A. G. *Organometallics* **1997**, *16*, 4581.
(32) Cornehl, H. H.; Wesendrup, R.; Diefenbach, M.; Schwarz, H. *Chem.—Eur. J.* **1997**, *3*, 1083.
(33) Schilling, J. B.; Beauchamp, J. L. *J. Am. Chem. Soc.* **1988**, *110*, 15.
(34) Sunderlin, L. S.; Armentrout, P. B. *J. Am. Chem. Soc.* **1989**, *111*, 3845.
(35) Heinemann, C.; Schroder, D.; Schwarz, H. *Chem. Ber.* **1994**, *127*, 1807.
(36) Cornehl, H. H.; Heinemann, C.; Schroder, D.; Schwarz, H. *Organometallics* **1995**, *14*, 9927.
(37) Gibson, J. K. *J. Phys. Chem.* **1996**, *100*, 15688.
(38) Santos, M.; Marcalo, J.; de Matos, A. P.; Gibson, J. K.; Haire, R. G. *J. Phys. Chem. A* **2002**, *106*, 7190.
(39) Santos, M.; Marcalo, J.; Leal, J. P.; de Matos, A. P.; Gibson, J. K.; Haire, R. G. *Int. J. Mass Spectrom.* **2003**, *228*, 457.
(40) Gibson, J. K.; Haire, R. G.; Marcalo, J.; Santos, M.; de Matos, A. P.; Leal, J. P. *J. Nucl. Mater.* **2005**, *344*, 24.
(41) Gibson, J. K.; Haire, R. G.; Santos, M.; Marcalo, J.; de Matos, A. P. *J. Phys. Chem. A* **2005**, *109*, 2768.
(42) Santos, M.; de Matos, A. P.; Marcalo, J.; Gibson, J. K.; Haire, R. G.; Tyagi, R.; Pitzer, R. M. *J. Phys. Chem. A* **2006**, *110*, 5751.
(43) Hay, P. J.; Martin, R. L. *J. Chem. Phys.* **1998**, *109*, 3875.
(44) Schreckenbach, G.; Hay, P. J.; Martin, R. L. *Inorg. Chem.* **1998**, *37*, 4442.
(45) Schreckenbach, G.; Hay, P. J.; Martin, R. L. *J. Comput. Chem.* **1999**, *20*, 70.
(46) Hay, B. P.; Nicholas, J. B.; Feller, D. *J. Am. Chem. Soc.* **2000**, *122*, 10083.
(47) Hay, P. J.; Martin, R. L.; Schreckenbach, G. *J. Phys. Chem. A* **2000**, *104*, 6259.
(48) Tuan, D. F. T.; Pitzer, R. M. *J. Phys. Chem.* **1996**, *100*, 6277.
(49) Zhang, Z. Y.; Pitzer, R. M. *J. Phys. Chem. A* **1999**, *103*, 6880.
(50) Matsika, S.; Pitzer, R. M. *J. Phys. Chem. A* **2000**, *104*, 4064.
(51) Matsika, S.; Pitzer, R. M. *J. Phys. Chem. A* **2001**, *105*, 637.
(52) Matsika, S.; Zhang, Z.; Brozell, S. R.; Baudeau, J. P.; Wang, Q.; Pitzer, R. M. *J. Phys. Chem. A* **2001**, *105*, 3825.
(53) Sonnenberg, J. L.; Hay, P. J.; Martin, R. L.; Bursten, B. E. *Inorg. Chem.* **2005**, *44*, 2255.
(54) Cao, Z. J.; Balasubramanian, K. *J. Chem. Phys.* **2005**, 123.
(55) Majumdar, D.; Balasubramanian, K.; Nitsche, H. *Chem. Phys. Lett.* **2002**, *361*, 143.
(56) Wheaton, V.; Majumdar, D.; Balasubramanian, K.; Chauffe, L.; Allen, P. G. *Chem. Phys. Lett.* **2003**, *371*, 349.
(57) Chaudhuri, D.; Balasubramanian, K. *Chem. Phys. Lett.* **2004**, *399*, 67.
(58) Wimmer, H.; Klenze, R.; Kim, J. I. *Radiochim. Acta* **1992**, *56*, 79.
(59) Kim, J. I.; Klenze, R.; Wimmer, H.; Runde, W.; Hauser, W. *J. Alloys Compd.* **1994**, *213*, 333.
(60) Fanghanel, T.; Weger, H. T.; Konnecke, T.; Neck, V.; Paviet-Hartmann, P.; Steinle, E.; Kim, J. I. *Radiochim. Acta* **1998**, *82*, 47.
(61) Fanghanel, T.; Weger, H. T.; Schubert, G.; Kim, J. I. *Radiochim. Acta* **1998**, *82*, 55.
(62) Klenze, R.; Panak, P.; Kim, J. I. *J. Alloys Compd.* **1998**, *271*, 746.
(63) Aas, W.; Steinle, E.; Fanghanel, T.; Kim, J. I. *Radiochim. Acta* **1999**, *84*, 85.
(64) Parr, R. G.; Yang, W. *Density Functional Theory of Atoms and Molecules*; Oxford: New York, 1989.
(65) Møller, C.; Plesset, M. *Phys. Rev.* **1943**, *46*, 618.
(66) Becke, A. D. *J. Chem. Phys.* **1993**, *98*, 5648.
(67) Vosko, S. H.; Wilk, L.; Nusair, M. *Can. J. Phys.* **1980**, *58*, 1200.
(68) Lee, C. T.; Yang, W. T.; Parr, R. G. *Phys. Rev. B* **1988**, *37*, 785.
(69) Nash, C. S.; Bursten, B. E.; Ermler, W. C. *J. Chem. Phys.* **1997**, *106*, 5133.
(70) Pacios, L. F.; Christiansen, P. A. *J. Chem. Phys.* **1985**, *82*, 2664.
(71) Cao, X. Y.; Dolg, M.; Stoll, H. *J. Chem. Phys.* **2003**, *118*, 487.
(72) Kuchle, W.; Dolg, M.; Stoll, H.; Preuss, H. *J. Chem. Phys.* **1994**, *100*, 7535.
(73) Duijneveldt, V. *IBM Tech. Res. Rep. RF1971*, 945.
(74) Frisch, M. J. *Gaussian 03*, revision C.02; Gaussian, Inc.: Pittsburgh, PA, 2005.
(75) Balasubramanian, K. *ALCHEMY*, Modified Version; 2002, Original authors of ALCHEMY II are M. Yoshimine, B. Lengsfiled, and B. Liu.
(76) Balasubramanian, K. *J. Chem. Phys.* **1988**, *89*, 5731.
(77) Köhler, S.; Diessenberger, R.; Eberhardt, K.; Erdmann, N.; Herrmann, G.; Huber, G.; Kratz, J. V.; Nunnemann, M.; Passler, G.; Rao, P. M.; Riegel, J.; Trautmann, N.; Wendt, K. *Spectrochim. Acta B* **1997**, *52*, 717.
(78) Blaise, J.; Wyart, J. F. *Energy Levels and Atomic Spectra of Actinides*; Paris, 1992; http//www.lac.u.psud.fr/Database/Contents.html.
(79) Balasubramanian, K. *Relativistic Effects in Chemistry Part A and B*; Wiley-Interscince: New York, NY, 1997.
(80) Balasubramanian, K.; Sikehaus, W.; McLean, W. *J. Chem. Phys.* **2003**, *119*, 5889.
(81) Balasubramanian, K.; Balazs, B.; McLean, W. *Chemtracts* **2006**, *19*, 66–77.
(82) Balasubramanian, K.; Felter, T. E.; Anklam, T.; Trelenberg, T. W.; McLean II, W. *J. Alloys Compd.* **2007**, 444–445,447.
(83) Balasubramanian, K.; Sikehaus, W.; McLean, W. *Uranium: Compounds, Isotopes and Applications*; Wolfe, G. H., Ed.; Nova Science Publishers: New York, NY, 2009.
(84) Yang, T.; Pitzer, R. M., Private Communications.

JP903795Q